CrossMark

ORIGINAL PAPER

Correlating annealing temperature of ZnO nanoparticle electron transport layer with performance of inverted polymer solar cells

Rui Xu[1] · Xiaoxiang Sun[1] · Chang Li[1] · Like Huang[1] ·
Zhenglong Li[1] · Hongkun Cai[1] · Juan Li[1] · Yaofang Zhang[2] ·
Jian Ni[1] · Jianjun Zhang[1]

Abstract We fabricated inverted polymer solar cells (PSCs) with the structure of ITO/ZnO NPs/Active layer/MoO$_3$/Ag, in which ZnO NPs act as electron transport layer (ETL), poly{4,8-bis[(2-ethylhexyl)oxy]benzo[1,2-b:4,5-b0]-dithiophene-2,6-diyl-alt-3-fluoro-2-[(2-ethylhexyl)carbonyl]thieno[3,4-b]thiophene-4,6-diy (PTB7) as donor and [6,6]-phenyl-C$_{71}$-butyric-acidmethyl-ester (PC$_{71}$BM) as accepter. It is found that the temperature employed during the annealing process of ZnO NPs has significant impact on the efficiency of the resulted PSCs. The optimized PSC with ZnO NPs annealed at 150 °C based on PTB7:PC$_{71}$BM (1:1.5 w/w) exhibited a power-conversion efficiency of 7.37% with open-circuit voltage (V_{oc}) of 0.722 V, short-circuit current density (J_{sc}) of 15.38 mA cm^{-2}, and fill factor (FF) of 66.4%. The effects of the annealing temperature on photovoltaic performances were further illustrated with transmission spectrum, atomic force microscopy, X-ray diffraction and PL spectra, meanwhile electrical performance were illustrated with conductivity. Our result indicated that the improved efficiency is due to the optimized ETL/active layer interface, the enhanced transparency and electron transport of the ETLs. As its facile preparation process, this kind of ETL is compatible with roll-to-roll manufacturing of larger area flexible PSCs.

Keywords Electron transport layer · ZnO nanoparticles · Annealing temperature · Polymer solar cell

✉ Jian Ni
  nijian_nankai@163.com

[1] The Tianjin Key Laboratory for Optical-Electronic Thin Film Devices and Technology, College of Electronic Information and Optical Engineering, Nankai University, Tianjin 300071, China

[2] College of Science, Tianjin Polytechnic University, Tianjin 300387, China

Introduction

Due to the potential for low-cost energy harvesting and flexibility application, extensive efforts have been directed at developing bulk heterojunction (BHJ) polymer solar cells (PSCs) [1–3]. The major challenges for BHJ solar cells are the achievement of competitive power-conversion efficiencies (PCEs) and the demonstration of long-term air stability [4–13]. Conventional PSCs are fabricated with a transparent conductive anode (e.g., indium tin oxide, ITO) and a low-work-function metal cathode (e.g., Al, Ca). However, metals with a low-work function are always susceptible to atmospheric oxidation [14]. Poly(3,4-ethylenedioxythiophene):poly(styrene sulfonate) (PEDOT:PSS) is often used as an anode buffer layer in the meantime. But PEDOT:PSS is hygroscopic and acidic, making it difficult to achieve long-term stability [15–19]. Aiming to eliminate this negative influence, inverted PSCs have been developed. Air-stable high-work-function metals (e.g., Au, Ag) are used as the anode, meanwhile n-type metal oxides such as titanium oxide (TiO_x) and zinc oxide (ZnO) are deposited onto the ITO electrode, working as electronic transport layer (ETL) [4]. In particular, ZnO is currently the most widely used ETL because of its fundamental and technological advantages: high optical transparency, high electron mobility, environmental stability and solution process ability [20, 21]. Therefore, solution-processed ZnO nanoparticles are used as ETL in PSCs, which can enhance the operational stability of PSCs by blocking the UV-light-induced photo degradation of organic materials [22]. It is known that up to 30% of the atomic bonds in ZnO NPs are dangling bonds and these defects give rise to a high density of recombination centers resulting in low power-conversion efficiencies in these inverted cells [23–25]. In this paper, we found that these defect states are sensitive to annealing temperature. By adjusting the annealing temperature of ZnO NP thin films, the device performance could be optimized. Furthermore, this kind of ZnO nanoparticles solution can stay stable in ambient air for a month, which simplifies the fabrication of polymer solar cells. We investigated the influence of the ZnO NP thermal annealing temperature on the photovoltaic performance of the devices in detail by adopting various annealing temperatures to fabricate the ZnO NP films. PCE up to 7.37% has been reached when the electron transport layer was annealed at optimized temperature of 150 °C in inverted PSC. To elucidate the mechanism of the influence of the annealing temperature on the performance of the inverted PSCs, samples were fabricated and characterized by transmission spectrum, atomic force microscopy, X-ray diffraction, PL and so on were used. And photovoltaic devices were characterized by external quantum efficiency (EQE) and current–voltage (I–V) measurements. Therefore, a low temperature annealing process for ZnO NPs are established, which make it possible to develop large area polymer solar cells on flexible substrates.

Experimental

The PSCs were fabricated with inverted structure of ITO/ZnO NPs/active layer/ MoO$_3$/Ag, as shown in Fig. 1a. The chemical structures of PTB7 and PC$_{71}$BM are shown in Fig. 1b. The patterned indium tin oxide (ITO) glass substrates with a low sheet resistance of about 15 Ω square^{-1} were cleaned in detergent, water, acetone, and isopropyl alcohol under ultra-sonication for 20 min, sequentially [26]. After ultraviolet/ozone treatment for 20 min, a thin layer ($\sim$ 30 nm) of ZnO NPs ETL was prepared through spin-coating of ZnO NP solution at 3000 rpm [27]. Then, the ZnO NP covered substrates were treated without annealing or with 100, 150 and 200 °C for 20 min in air, respectively. The PTB7 and PC$_{71}$BM (1:1.5 w/w) were co-dissolved in the solvent of CB, and 3% volume ratio of 1,8-diiodooctane (DIO) was added as a processing additive before use [1]. The polymer concentration was 10 mg mL^{-1} and the solution was stirred at 60 °C for 12 h under an N$_2$ environment. Then the active layer ($\sim$ 100 nm) was deposited on the ZnO NPs layer by spin-coating the as-prepared solutions at 1500 rpm for 30 s in N$_2$-filled glovebox. Finally, a 7-nm thick MoO$_3$ layer and a 100-nm thick Ag layer were subsequently evaporated through a shadow mask (active area 6 mm^2) under the pressure of 7.0×10^{-4} Pa to finish the device fabrication [26]. The chemical synthesis of ZnO nanoparticles was performed using the method outlined by Sun et al. [28]. Briefly, zinc acetate (2.97 g) was added to methanol (125 mL) under vigorous stirring at about 60 °C. Subsequently, a solution of KOH (1.51 g) in methanol (65 mL) was dissolved in the solution. The reaction mixture was stirred for 2 h at 60 °C [29].

The current density–voltage (J–V) characteristics of the devices were measured under 1-sun (AM 1.5G, 100 mW cm^{-2}) simulator radiation [26]. The EQE spectra were measured using a Solar Cell Quantum Efficiency Measurement System (QEX10) from PV Measurements, Inc. The transmittance spectrum of the ZnO nanoparticle thin films were measured by spectrophotometer (Cary 5000 UV–VIS). X-ray diffraction measurements were carried out using a Philips X'pert Pro diffractometer with Cu-Kα radiation at 45 kV and 40 mA. Transmission electron microscopy (TEM) image was obtained using a Hitachi TEM system, the ZnO
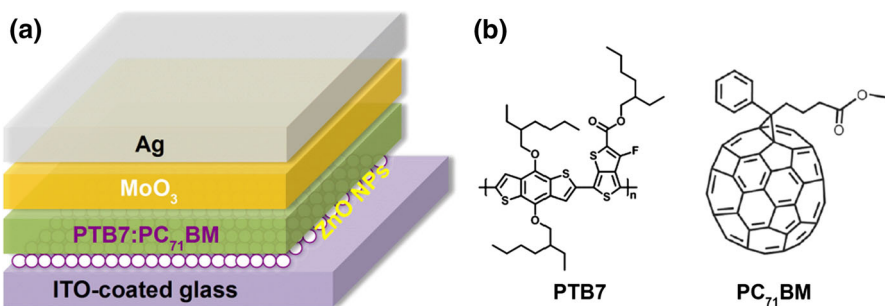

Fig. 1 a Device architecture of the inverted polymer solar cells with the ZnO NPs buffer layer. b Chemical structures of PTB7 and PC$_{71}$BM

nanoparticle solutions were dropped on a holey carbon-coated copper grid. The perpendicular electrical properties of the ZnO NP thin films were measured through a sandwich structure of ITO/ZnO NPs/Ag [26]. The surface morphology was observed by AFM (Seiko SPA-400 SPM UNIT). Photoluminescence (PL) spectrometer was used to measure the emission spectra of the blend films. The X-ray photoelectron spectroscopy (XPS) measurements were performed with a Thermo Scientific ESCALAB 250Xi. ZnO NP films were deposited on top of ITO substrates by spin casting in air. For XPS data, curve fitting and linear background subtraction were done using Thermo Avantage software.

Results and discussion

The XRD patterns of the prepared ZnO nanoparticle samples we fabricated are shown in Fig. 2. All the detectable peaks could be indexed as the ZnO wurtzite structure found in the standard reference data (JCPDS: 36e1451) [30]. It was clearly seen that the diffraction peaks were sharp, indicating the great crystallinity of the ZnO NPs. The inset picture in Fig. 1 displays the TEM image of the ZnO NPs, which can show that the diameter of ZnO nanoparticles is approximately 5 nm.

To evaluate the effect of the annealing temperature on the performance of the cells, we fabricated PSCs incorporating ZnO NP films annealed at various temperature with the same duration [31]. The $J–V$ characteristics of the devices, incorporating ZnO NPs films annealed at different temperatures under AM 1.5 G irradiation with irradiation intensity of 100 mW cm^{-2} are shown in Fig. 3a. Table 1
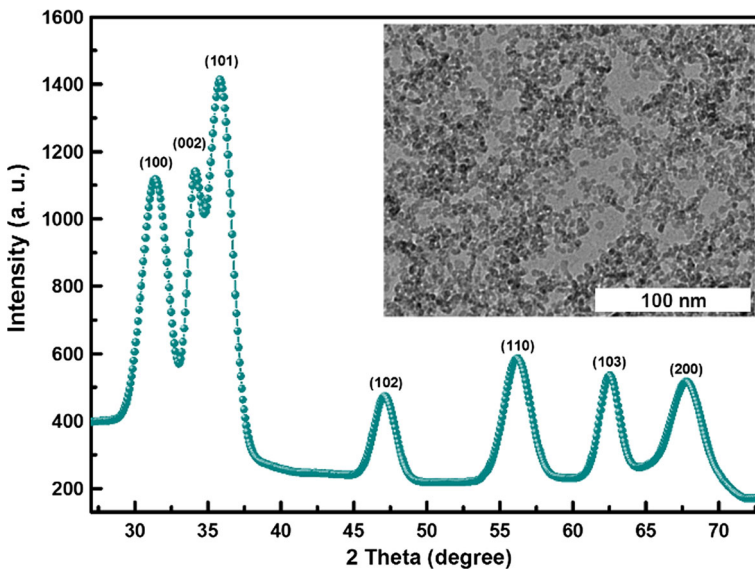
Fig. 2 X-ray diffraction (XRD) spectra of ZnO nanoparticles powder. The inset picture is a TEM image of the ZnO nanoparticles
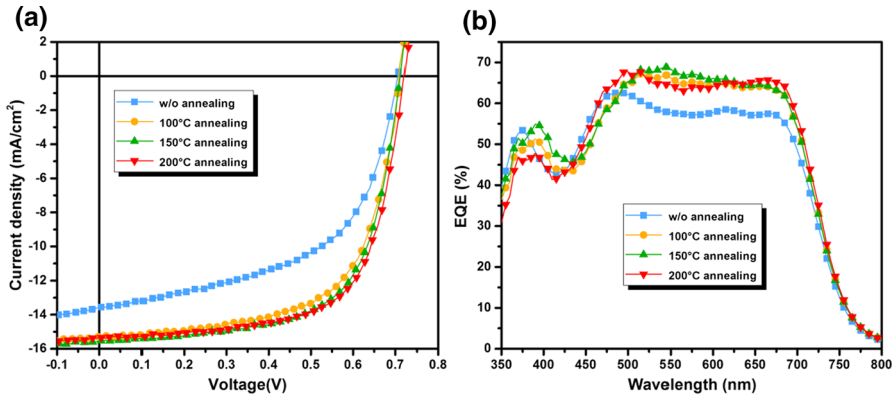
Fig. 3 **a** *J–V* characteristics of inverted PTB7:PC$_{71}$BM solar cells incorporating ZnO nanoparticles films with or without annealing treatment. **b** The external quantum efficiency (EQE) spectra of the corresponding devices

Table 1 The parameters of the BHJ solar cells prepared with various annealing temperature of ZnO NPs ETL

Temperature (°C)	V_{oc} (V)	J_{sc} (mA cm^{-2})	FF (%)	PCE (%)	R_S (Ω cm^2)	R_{SH} (Ω cm^2)	Calculated J_{sc} (mA cm^{-2})
w/o	0.706	13.41	54.92	5.20	6.17	606.044	12.77
100	0.711	15.15	63.86	6.88	4.36	765.997	13.77
150	0.722	15.38	66.39	7.37	5.90	1157.873	13.98
200	0.712	15.24	65.04	7.06	5.45	1117.74	13.91

summarizes the extracted photovoltaic parameters of the devices. The value of J_{sc} has been cross-checked with the integral of external quantum efficiency spectrum (shown in Fig. 3b) and the results are within 10% error. Obvious differences are found in device performance when ZnO NP films were annealed at various temperature. As shown in Table 1, the device utilizing ZnO NPs without annealing treatment as ETL shows worse performance (V_{oc} = 0.706 V, J_{sc} = 13.41 mA cm^{-2}, FF = 54.92% and PCE = 5.20%), which confirms the necessity of annealing for high quality ZnO NPs. The performance of devices improved after anneal treatment of ETLs. The device corresponding to 100 °C annealing shows V_{oc} = 0.711 V, J_{sc} = 15.15 mA cm^{-2}, FF = 63.86% and PCE = 6.88%. When compared with the performance of the inverted devices annealed at 100 °C, device annealed at 150 °C (V_{oc} = 0.722 V, J_{sc} = 15.38 mA cm^{-2}, FF = 66.39% and PCE = 7.37%) shows improved V_{oc}, J_{sc} and FF, which is indicative of efficient photon-to-electron conversion. Nevertheless, as the annealing temperature was further increased to 200 °C, degradation happens to the performance of the inverted organic solar cells. The V_{oc} reduces from 0.722 to 0.712 V, J_{sc} decreases from 15.38 to 15.24 mA cm^{-2}, FF decreases from 66.39 to 65.04%, and PCE drops from 7.37

to 7.06% when the temperature increased from 150 to 200 °C. We report the EQE of the series of device in Fig. 3b. The device shows a broad response range from 350 to 800 nm (according to the one of the conventional device reported in the literature [32]), with values greater than 65% in the range 500–700 nm. The value slightly decreases when the annealing temperature is below or above 150 °C. Moreover, there is a clear decline in EQE values of samples without annealing treatment, which confirms that the thermal annealing is necessary for high-quality ZnO NPs and high-performance polymer solar cells.

The optical properties of the ZnO NP films produced with different annealing temperature were investigated by collecting their transmittance spectra, as reported in Fig. 4. All ZnO NP thin films showed comparable optical properties over the entire visible wavelength range with an average optical transmittance of about 92%, which is better than the transmittance of 7059 glass. As the annealing temperature rises, the transmittance becomes higher on the range of 370–800 nm. It indicates a limited parasitic absorption that could negatively affect charge generation in the photoactive layer. Therefore, the annealing temperature of ZnO NPs can significantly improve the optical absorption properties of the active layer thus the photovoltaic performance of the devices [33]. The result of transmittance spectra indicates that the annealing treatment can effectively enhance the optical transmittance of the ETL. However, it is worth emphasizing that the optical transmittance of the ZnO NP layer is different from the optical transmittance of the entire device. The structure of entire device is more complex and requires the subsequent deposition of the active layer, MoO_3 HTL and Ag electrode. We believe that the more complex structure and optical propagation in the entire device may lead to changes in the distribution of light intensity in the active layer, resulting in inconsistent results of EQE and transmittance in the wavelength range of
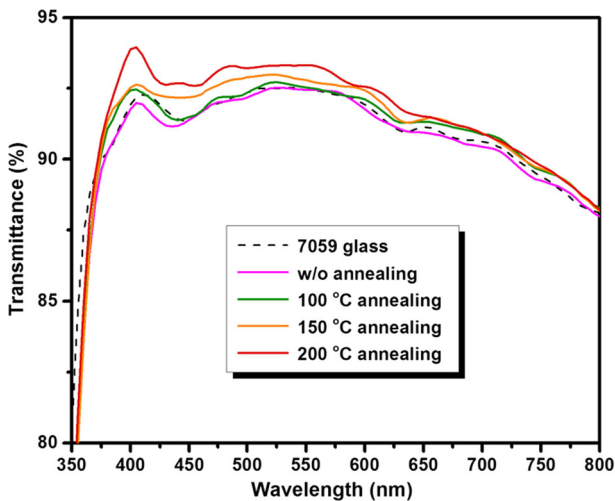

Fig. 4 Transmittance spectrum of the ZnO nanoparticles layers deposited on 7059 glass substrate and annealed at different temperature

350–425 nm. In addition, the property reduction of the front interface mainly affected the light response of the short wavelength range.

To further study the diversification of the electrical properties by the changing of annealing temperature, here we introduce the perpendicular electrical transport behaviors, as shown in Fig. 5. ZnO NP thin film without annealing shows worse conductivity. The dark conductivities of ZnO NPs thin film are improved with the increase of annealing temperature from 100 to 150 °C, which can be attributed to a better transport of the electrons due to suitable annealing treatment that can effectively remove surface defects and thus better electrical contact between ZnO NPs is ensured. To intuitively figure out the conductive properties, we calculated the resistance and conductance of ZnO NP films shown as Table 2. When the annealing temperature was up to 150 °C, the conductivity of ZnO NP films is 1.882×10^{-5} s cm^{-1}, which shows a better electrical performance relatively. However, as the temperature continuing rise to 200 °C, the conductivity reduced to as low as the samples without annealing. In this case, 150 °C is the optimized treatment temperature beneficial for the best electrical performance of device.

To figure out the mechanism behind the effect of annealing temperature on the quality of ZnO NPs, the nanoscale surface morphologies and surface roughness of the ZnO NP thin films annealed at different temperature were investigated by atomic force microscopy (AFM). Figure 6a–d shows the topography AFM images for ZnO NP films. Obviously, the annealing temperature of the ZnO NP films could affect its roughness. The surface root mean square (RMS) roughness values are 4.39, 3.53, 2.86 and 3.44 nm for ZnO NP films without annealing, annealed at 100, 150 and 200 °C, respectively. It is clear that the ZnO NP films via the 150 °C annealing treatment possesses a better morphology as its surface is smoother, indicating that the voids between the ZnO nanoparticles were effectively reduced [34]. Such a uniform and smooth surface is expected to enable a good contact
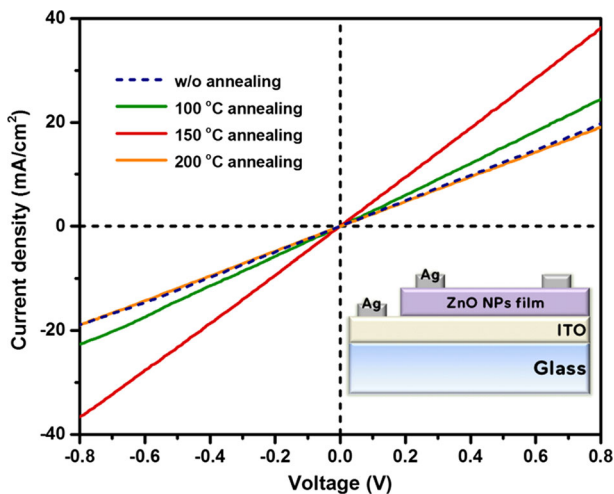
Fig. 5 The perpendicular electrical transport behaviors for ZnO NPs thin films with different annealing temperature. The inset picture is the structure of the device

Table 2 The resistance and conductivity of ZnO NP film

Temperature (°C)	w/o	100	150	200
R (Ω)	690.703	567.086	354.157	700.574
σ (s cm^{-1})	9.652×10^{-6}	1.176×10^{-5}	1.882×10^{-5}	9.516×10^{-6}
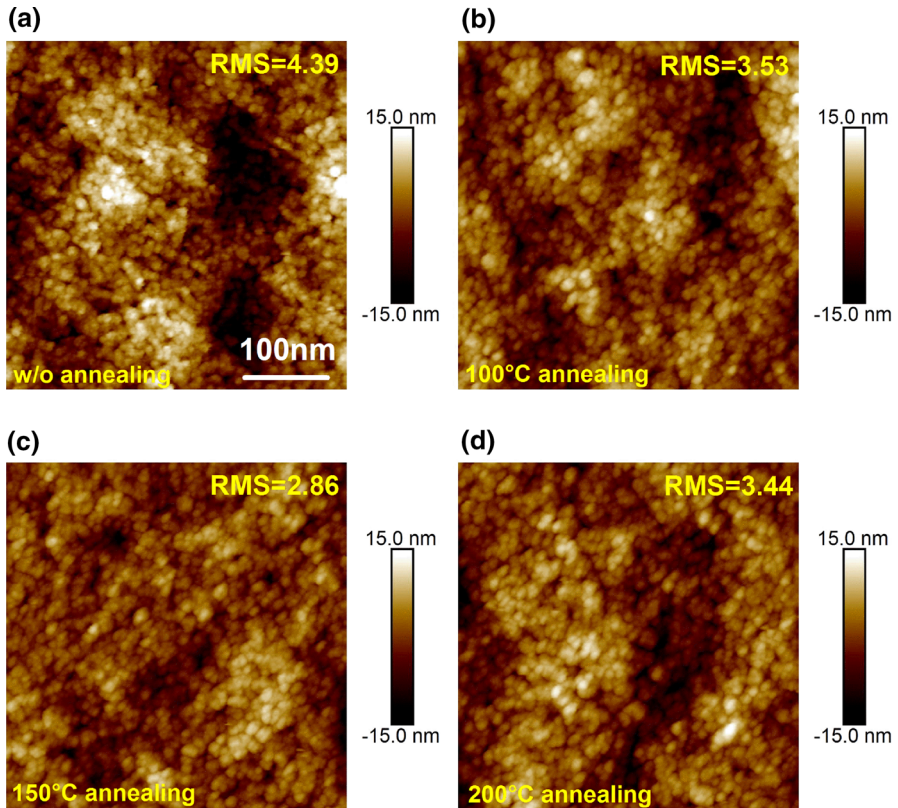
Fig. 6 AFM images of ZnO nanoparticles films with the following annealing treatment: **a** without annealing, **b** 100 °C, **c** 150 °C, **d** 200 °C

between the ETL and the PTB7:PC$_{71}$BM layer for the device with the ZnO NPs ETL [35], which reduces photocarrier recombination loss enormously during electron transport process. The growth in number of interface traps increased the possibility of trap-assisted recombination of the electrons, leading to the low FF and thus the poor PCE of the device, which is consistent with the results shown in Table 1. Therefore, the better electron collection efficiency in the device with the ZnO NP ETL annealed at 150 °C yields a significantly increased EQE, bringing about a higher J_{sc}, and the effectively suppressed trap-assisted recombination

contributes to an enhanced FF, both of which undoubtedly result in the improvement in performance [36]. Therefore, greater homogeneity can be observed in the photoactive layer deposited on top of the ZnO NP interlayer when annealing temperature is 150 °C. The enhanced device performance with annealed ZnO NP films is believed to be attributed to the modified surface composition promoting charge collection.

For further explanation of the device's phenomena, the XPS measurements were carried out. The XPS spectra were conducted to explore the nature of the surface defects of the ZnO NP layers, which are presented in Fig. 7. It shows core-level XPS spectra of Zn 2p and O 1s for the ZnO NP films unannealed and annealed at 150 °C. From Fig. 7a, the binding energy of Zn $2p_{3/2}$ peak was at 1021.5 eV for the ZnO films without annealing [37–39]. The maximum of the Zn $2p_{3/2}$ peak shifts toward lower binding energy by 0.1 eV as the annealing temperature is increased up to 150 °C; the shift implies that more Zn atoms are bound to O atoms. The O 1s spectra specimens were found to consist of two components as shown in Fig. 7b. The peak with lower binding energy (530.1 eV) corresponds to O atoms in a ZnO matrix. The higher-binding energy component at 532.7 eV is attributed to chemisorbed oxygen [40]. The main peak shifts towards lower energy by 0.2 eV after annealing at 150 °C. From the decreased intensity of the higher-binding energy component, we infer that the oxygen-deficient component decreases with annealing. Therefore, 150 °C annealing treatment decreases the oxygen-deficient component and increases the number of Zn–O bonds in the ZnO NP film [4]. The result indicates that 150 °C annealing treatment can reduce the concentration of oxygen vacancies in the ZnO film, decreasing the number of electron traps and the probability of charge recombination [36].

Photoluminescence (PL) spectra were performed on a HITACHI visible-ultraviolet spectrophotometer with a Xe lamp as the excitation light source at room temperature. The excited wavelength was 610 nm. The PL measurements for active layer with ZnO nanoparticles are performed to explore the electron transfer characteristics at the active layer/ZnO NP interface as shown in Fig. 8. The PL spectrum patterns (Fig. 8) for ZnO/PTB7:PC$_{71}$BM assemblies consist of a strong
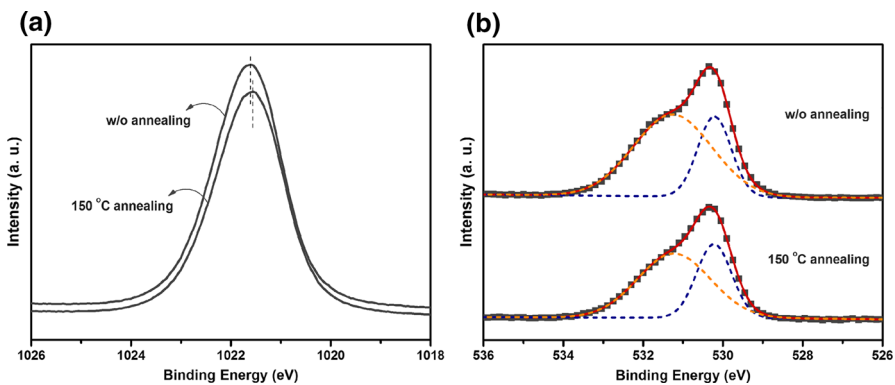
Fig. 7 a Zn 2p and b O 1s XPS spectra of ZnO NPs films with different annealing temperature
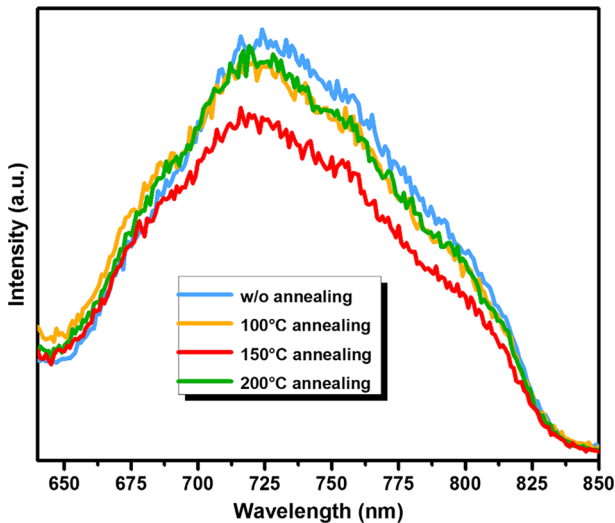
Fig. 8 PL spectra of ITO/ZnO NPs/PTB7:PC$_{71}$BM samples with ZnO NPs annealed at different temperature

emission band peak at around 725 nm. The luminescence intensity decreases with the increase of thermal treatment temperature up to 150 °C, then it was enhanced to be almost the same as that of the samples treated at 100 °C as the temperature was further increased to 200 °C. The diversification of PL intensity indicated that the surface defects were restrained and repaired by thermal treatment with ETL, which is accordance with the results of AFM images. In the photovoltaic device, the reduction of traps can decrease the possibility of trap-assisted interfacial recombination of carriers and consequently enhance J_{sc} and FF of the device. Thus, the PCE of device was improved [41]. The suitable increasing of annealing temperature for ETL could enhance electron transfer quality between active layer and ETL and improve the performance of the device.

Conclusions

In this work, we reported the application of ZnO NP thin film as an electron transport layer for efficient and air-stable inverted PSCs based on a blend film of PTB7:PC$_{71}$BM. Power-conversion efficiency of 7.37% is demonstrated simply by optimizing the annealing temperature of ZnO NPs. ZnO NP layer annealed at 150 °C shows most effective performance in collecting electrons from PC$_{71}$BM. To figure out the mechanism behind the effect of annealing temperature on the quality of ZnO NPs, transmittance spectrum, dark conductivity, AFM, XPS and PL measurement were conducted. Studies on film morphology suggest that the 150 °C annealed ZnO NPs ETL is characterized by a notably smooth and compact surface. It is found that the optimized annealing temperature can reduce surface defect and improve surface morphology thus the conductivity of the ZnO NP layer, inducing a

better electron transfer between active layer and ETL and improved electron transport of ETL. The annealing temperature applied here to treat the ZnO NP film is compatible with flexible substrates and the results define a promising pathway for fabrication of efficient lager area polymer solar cells in a low energy consumption thus low-cost manner.

References

1. Small CE, Chen S, Subbiah J, Amb CM, Tsang S-W, Lai T-H, Reynolds JR, So F (2012) High-efficiency inverted dithienogermole-thienopyrrolodione-based polymer solar cells. Nat Photonics 6:115
2. Li G, Chu C-W, Shrotriya V, Huang J, Yang Y (2006) Efficient inverted polymer solar cells. Appl Phys Lett 88:253503
3. Chen LM, Hong Z, Li G, Yang Y (2009) Recent progress in polymer solar cells: manipulation of polymer: fullerene morphology and the formation of efficient inverted polymer solar cells. Adv Mater 21:1434
4. Sun Y, Seo JH, Takacs CJ, Seifter J, Heeger AJ (2011) Inverted polymer solar cells integrated with a low-temperature-annealed sol–gel-derived ZnO film as an electron transport layer. Adv Mater 23:1679
5. Liang Y, Yu L (2010) A new class of semiconducting polymers for bulk heterojunction solar cells with exceptionally high performance. Acc Chem Res 43:1227
6. Park SH, Roy A, Beaupré S, Cho S, Coates N, Moon JS, Moses D, Leclerc M, Lee K, Heeger AJ (2009) Bulk heterojunction solar cells with internal quantum efficiency approaching 100%. Nat Photonics 3:297
7. Blouin N, Michaud A, Gendron D, Wakim S, Blair E, Neagu-Plesu R, Belletete M, Durocher G, Tao Y, Leclerc M (2008) Toward a rational design of poly(2,7-carbazole) derivatives for solar cells. J Am Chem Soc 130:732
8. Ma W, Yang C, Gong X, Lee K, Heeger AJ (2005) Thermally stable, efficient polymer solar cells with nanoscale control of the interpenetrating network morphology. Adv Funct Mater 15:1617
9. Li G, Shrotriya V, Huang J, Yao Y, Moriarty T, Emery K, Yang Y (2005) High-efficiency solution processable polymer photovoltaic cells by self-organization of polymer blends. Nat Mater 4:864
10. Peet J, Kim JY, Coates NE, Ma WL, Moses D, Heeger AJ, Bazan GC (2007) Efficiency enhancement in low-bandgap polymer solar cells by processing with alkane dithiols. Nat Mater 6:497
11. Hauch JA, Schilinsky P, Choulis SA, Childers R, Biele M, Brabec CJ (2008) Flexible organic P3HT: PCBM bulk-heterojunction modules with more than 1 year outdoor lifetime. Sol Energy Mater Sol Cells 92:727
12. Lungenschmied C, Dennler G, Neugebauer H, Sariciftci SN, Glatthaar M, Meyer T, Meyer A (2007) Flexible, long-lived, large-area, organic solar cells. Sol Energy Mater Sol Cells 91:379
13. Brabec CJ, Gowrisanker S, Halls JJ, Laird D, Jia S, Williams SP (2010) Polymer–fullerene bulk-heterojunction solar cells. Adv Mater 22:3839
14. Hung L, Tang CW, Mason MG (1997) Enhanced electron injection in organic electroluminescence devices using an Al/LiF electrode. Appl Phys Lett 70:152
15. Kawano K, Pacios R, Poplavskyy D, Nelson J, Bradley DD, Durrant JR (2006) Degradation of organic solar cells due to air exposure. Sol Energy Mater Sol Cells 90:3520
16. De Jong M, Van Ijzendoorn L, De Voigt M (2000) Stability of the interface between indium-tin-oxide and poly(3,4-ethylenedioxythiophene)/poly (styrenesulfonate) in polymer light-emitting diodes. Appl Phys Lett 77:2255
17. Jørgensen M, Norrman K, Krebs FC (2008) Stability/degradation of polymer solar cells. Sol Energy Mater Sol Cells 92:686

18. Yan H, Lee P, Armstrong NR, Graham A, Evmenenko GA, Dutta P, Marks TJ (2005) High-performance hole-transport layers for polymer light-emitting diodes. Implementation of organosiloxane cross-linking chemistry in polymeric electroluminescent devices. J Am Chem Soc 127:3172

19. Norrman K, Gevorgyan SA, Krebs FC (2008) Water-induced degradation of polymer solar cells studied by $H_2^{18}O$ labeling. ACS Appl Mater Interfaces 1:102

20. Krebs FC (2009) All solution roll-to-roll processed polymer solar cells free from indium-tin-oxide and vacuum coating steps. Org Electron 10:761

21. Desai A, Haque M (2007) Mechanical properties of ZnO nanowires. Sens Actuators A 134:169

22. Yang T, Cai W, Qin D, Wang E, Lan L, Gong X, Peng J, Cao Y (2010) Solution-processed zinc oxide thin film as a buffer layer for polymer solar cells with an inverted device structure. J Phys Chem C 114:6849

23. Chen S, Small CE, Amb CM, Subbiah J, Lai Th, Tsang SW, Manders JR, Reynolds JR, So F (2012) Inverted polymer solar cells with reduced interface recombination. Adv Energy Mater 2:1333

24. Fonoberov VA, Alim KA, Balandin AA, Xiu F, Liu J (2006) Photoluminescence investigation of the carrier recombination processes in ZnO quantum dots and nanocrystals. Phys Rev B 73:165317

25. Klenk R (2001) Characterisation and modelling of chalcopyrite solar cells. Thin Solid Films 387:135

26. Sun X, Li C, Huang L, Xu R, Ni J, Cai H, Li J, Zhang J (2017) Effects of high-boiling-point additive 2-bromonaphthalene on polymer solar cells fabricated in ambient air. Polym Bull 74(11):4515–4524

27. Sun X, Ni J, Li C, Huang L, Xu R, Li Z, Cai H, Li J, Zhang J (2016) Air-processed high performance ternary blend solar cell based on PTB7-Th:PCDTBT:PC 70 BM. Org Electron 37:222

28. Sun B, Sirringhaus H (2005) Solution-processed zinc oxide field-effect transistors based on self-assembly of colloidal nanorods. Nano Lett 5:2408

29. Zak AK, Abrishami ME, Majid WA, Yousefi R, Hosseini S (2011) Effects of annealing temperature on some structural and optical properties of ZnO nanoparticles prepared by a modified sol–gel combustion method. Ceram Int 37:393

30. Zak AK, Majid WA, Abrishami ME, Yousefi R (2011) X-ray analysis of ZnO nanoparticles by Williamson-Hall and size–strain plot methods. Solid State Sci 13:251

31. Morvillo P, Diana R, Ricciardi R, Bobeico E, Minarini C (2015) High efficiency inverted polymer solar cells with solution-processed ZnO buffer layer. J Sol Gel Sci Technol 73:550

32. Chen H-Y, Hou J, Zhang S, Liang Y, Yang G, Yang Y, Yu L, Wu Y, Li G (2009) Polymer solar cells with enhanced open-circuit voltage and efficiency. Nat Photonics 3:649

33. Iannaccone G, Bernardi A, Suriano R, Bianchi CL, Levi M, Turri S, Griffini G (2016) The role of sol–gel chemistry in the low-temperature formation of ZnO buffer layers for polymer solar cells with improved performance. RSC Adv 6:46915

34. Wang G, Jiu T, Tang G, Li J, Li P, Song X, Lu F, Fang J (2014) Interface modification of ZnO-based inverted PTB7:PC71BM organic solar cells by cesium stearate and simultaneous enhancement of device parameters. ACS Sustain Chem Eng 2:1331

35. Lv L, Lu Q, Ning Y, Lu Z, Wang X, Lou Z, Tang A, Hu Y, Teng F, Yin Y (2014) Self-assembled TiO_2 nanorods as electron extraction layer for high-performance inverted polymer solar cells. Chem Mater 27:44

36. Huang X, Lv L, Hu Y, Lou Z, Hou Y, Teng F (2017) Enhanced performance in inverted polymer solar cells employing microwave-annealed sol–gel ZnO as electron transport layers. Org Electron 42:107

37. Chen M, Wang X, Yu Y, Pei Z, Bai X, Sun C, Huang R, Wen L (2000) X-ray photoelectron spectroscopy and auger electron spectroscopy studies of Al-doped ZnO films. Appl Surf Sci 158:134

38. Natsume Y, Sakata H (2000) Zinc oxide films prepared by sol–gel spin-coating. Thin Solid Films 372:30

39. Wan Q, Yu K, Wang T, Lin C (2003) Low-field electron emission from tetrapod-like ZnO nanostructures synthesized by rapid evaporation. Appl Phys Lett 83:2253

40. Islam MN, Ghosh T, Chopra K, Acharya H (1996) XPS and X-ray diffraction studies of aluminum-doped zinc oxide transparent conducting films. Thin Solid Films 280:20

41. Lee EJ, Heo SW, Han YW, Moon DK (2016) An organic–inorganic hybrid interlayer for improved electron extraction in inverted polymer solar cells. J Mater Chem C 4:2463